REPORT TO THE

NATIONAL AERONAUTICS AND SPACE ADMINISTRATION

- MARSHALL SPACE FLIGHT CENTER -

FINAL STATUS REPORT

for

GRANT NAG 8-829

A TECHNIQUE FOR MEASURING VERTICALLY AND HORIZONTALLY POLARIZED MICROWAVE BRIGHTNESS TEMPERATURES USING ELECTRONIC POLARIZATION-BASIS ROTATION

A.J. Gasiewski (Principal Investigator)

D.B. Kunkee

Covering the period from

June 1, 1990 to November 30, 1991

Submitted by:

Professor Albin J. Gasiewski
School of Electrical Engineering
Georgia Institute of Technology
Atlanta, Georgia, 30332-0250
(404) 894-2934

NASA Technical Officer:

Dr. Roy W. Spencer
Code ES43
NASA Marshall Space Flight Center
Marshall Space Flight Center, AL 35812
(205) 544-1686

TABLE OF CONTENTS

INTRODUCTION

A technique for electronically rotating the polarization basis of a dual orthogonal-linear polarization radiometer has been successfully demonstrated by investigators at the Georgia Institute of Technology. The technique is based on the measurement of the first three feedhorn Stokes parameters along with subsequent transformation of this measured Stokes vector into a rotated coordinate frame (Gasiewski, 1990; Parks, et al, 1988; see also Appendix A). The technique requires an accurate measurement of the cross-correlation between the two orthogonal feedhorn modes, for which an innovative polarized calibration load has been developed.

The electronic technique can simplify designs of satellite-based scanning polarized microwave imagers by electronically (rather than mechanically) rotating the polarization basis of the radiometer. For scanning imagers, some means of rotation is required in order that the feedhorn basis remain coincident with the Earth's vertical-horizontal basis throughout the entire scan. Potential applications include the Defense Meteorological Satellite Program (DMSP) microwave precipitation instruments, the TRMM Microwave Imager (TMI), the EOS Multifrequency Imaging Microwave Radiometer (MIMR), and airborne passive microwave radiometers for meteorological research.

The experimental portion of this investigation has consisted of a proof-of-concept demonstration of the technique of electronic polarization-basis rotation (EPBR) using a ground-based 90-GHz dual orthogonal-linear polarization radiometer. Practical calibration algorithms for ground-, aircraft-, and space-based instruments have been identified and tested. The theoretical effort has consisted of radiative transfer modeling using the planar-stratified numerical model described in Gasiewski and Staelin (1990).

SUMMARY OF ACTIVITIES

Activities sponsored by this grant at Georgia Tech during the period from June 1, 1990 to November 30, 1991 include acquisition of required hardware for the ground-based EPBR demonstration instrument, construction of all electrical and mechanical subsystems for the ground-based demonstration unit, development of practical calibration algorithms, ground-based experiments verifying the concept of EPBR, and radiative transfer calculations.

A. Hardware

Briefly, the demonstration instrument consists of a 90-GHz dual orthogonal-linear mode radiometer, modified to include an additional cross-correlating channel (Figure 1). The addition of this channel allows the orthogonal-linear polarization basis of the radiometer to be rotated by any desired angle. The radiometer is supplied by the NASA Goddard Space Flight Center, and will be available for use at Georgia Tech through March, 1992, and beginning again in June, 1992.

The cross-correlation channel is implemented as an adding correlator. Relatively little hardware beyond that required to implement a conventional dual-polarization radiometer (i.e., without cross-correlation channel) is required. This hardware consists of three microwave power divider/combiners, a video detector and a video summing amplifier. In order to measure the cross-correlating signal with minimal corruption by additive radiometric noise, the total gains (including IF, RF, and video) of all channels must be balanced, and the radiometric noise from the vertical and horizontal channels must be subtracted in the summing amplifier (Gasiewski 1990).

An adjustable local oscillator (LO) phase shifter was installed in one of the two LO-mixer paths to allow precise adjustment of the cross-correlation channel to measure either in-phase correlation (T_U) or quadrature correlation (T_V). The adjustable phase shifter provides the

capability to measure all four Stokes parameters by switching the LO phase by 90^{o}.

An IBM PS-2 Model 30 computer with a Keithley Metrabyte A/D converter, digital I/O system, and stepper motor drive capability was configured to provide temperature and radiometric data acquisition, instrument control, and calibration capabilities. The data acquisition and calibration software were developed at Georgia Tech.

The measured responses of the three channels to a linearly polarized CW source as a function of source polarization angle are shown in Figure 2. The data indicate good cross-correlation response, as seen by the 45-degree phase shift of the U-channel response relative to the A- and B-channels. Worst-case cross-polarization isolation for the A- and B-channels is approximately 15 dB. Although this is somewhat low, it appears to be acceptable for EPBR. (It is noted that a 15 degree offset in the electric field orientation relative to the instrument's window mounting plate at the co-polarized response maximum of the A-channel was observed. This is suspected to be caused by imperfect alignment of the radiometer's orthogonal-mode coupler. The misalignment is not serious for this investigation, since it remains constant. However, it should be accounted for by other investigators using the GSFC 90-GHz instrument.)

B. Calibration Algorithms

The radiometric response of all three channels must be known in order to interpret the measured output voltages. A polarized calibration load using hot and cold microwave absorbers and a polarization-splitting wire grid (Gasiewski, 1990; Figure 3) was constructed for this purpose. The configuration of the absorbers and grid were chosen to provide a precisely-known polarized Stokes field to the feedhorn of the radiometer. Observations of this load at several angles of rotation allowed the gains and offsets of all three channels (both orthogonal mode and cross-correlation) to be measured.

In calibrating the radiometer, four parameters must be determined for

each of the three channels: a primary gain, an offset, and two crosstalk gains. Although the crosstalk gains should be zero, in practice they are not and need to be determined for accurate EPBR. To determine the four unknown parameters, an invertible gain/offset observation matrix must be obtained for each channel. For example, let the output voltages of the U-channel for N calibration looks be given by the values v_i, and let the corresponding feedhorn Stokes' brightnesses be (T_{Ai}, T_{Bi}, T_{Ui}). These values are linearly related by the U-channel gains (g_{UA}, g_{UB}, g_{UU}) and offset o_U:

where n_i is a radiometric noise voltage. If the above matrix is rank four (i.e., full row rank) and the noise standard deviation is small, then a unique solution for the gains and offset exists. In principle, the radiometric noise can be reduced arbitrarily by increasing the integration time of the calibration look or (equivalently) averaging over a number of looks.

A rank-four observation matrix can be obtained using four calibration looks: three at the polarized load rotated to three appropriate angles (e.g., 0,45, and 90^{o}) and one at an additional unpolarized load. This scheme was found to most convenient for laboratory experiments, and was adopted. The additional view of an unpolarized load was accomplished by sliding a piece of room-temperature absorbing foam over the feedhorn.

The expected accuracies of several alternate schemes for calibrating the instrument were also investigated. The performance of each of these schemes was analyzed using the matrix software package MATLAB. Each scheme consists of a particular hardware configuration employing a polarized calibration load and/or an unpolarized load viewed in a particular calibration load viewing sequence. A calibration sequence consists of a series of views of either an unpolarized load or a polarized load rotated to predetermined angle.

Indeed, the best simulated results are achieved using a calibration scheme with a rank-four gain/offset observation matrix. Non full-rank observation matrices and/or noise-corrupted calibration looks are less desirable for measuring the channel gains and offsets. For example, if the calibration sequence is implemented by viewing only a simple two-temperature polarized load, the crosstalk gains can not be unambiguously determined. This is not to say that the crosstalk gains could not be statistically determined, but this would require a-priori statistical knowledge of the drift behavior of the hardware. Thus, the non-full rank schemes are highly specific to the radiometer hardware, and not generally recommended.

Thus, for airborne or spaceborne applications, a view of an unpolarized load (e.g., cold space) along with the simple two-temperature polarized load during the calibration cycle is nearly essential. However, a slightly more complicated three-temperature polarized load can provide nearly the same results without the necessity of viewing an unpolarized load. Only a polarizing wire grid need be rotated, thus minimizing mechanical complexity. (A splash plate would also have to be inserted to allow the feedhorn to view the calibration load.) This scheme would use one hot calibration load (viewed by the polarization transmitted through the wire grid) and two cold calibration loads (each viewed by the polarization reflected from the wire grid). One of these two cold loads would typically be an ambient-temperature blackbody (approximately 250 K), and the other could be cold space (2.73 K). A calibration sequence viewing both the hot/ambient and hot/space load combinations at appropriate angles of the rotating wire grid provide a full-rank gain/offset observation matrix. Since only the wire grid need be rotated, the rotating mass is minimal, and slip rings for electrical connections are unnecessary.

C. Ground-based Demonstration of EPBR

The ability to calibrate an EPBR radiometer and transform the feedhorn brightness temperatures into the natural basis was successfully demonstrated using outdoor observations of a reflecting water surface at

near-Brewster angle (65^{o}) incidence under clear-sky conditions. For the chosen incidence angle, the vertically and horizontally polarized brightnesses differ significantly (T_V~260 K, T_H~135 K), causing a high degree of polarization (m~0.32). A conically-scanning mirror was configured to sweep the radiometer beam across the water surface, thereby rotating the feedhorn polarization basis relative to the natural basis while maintaining constant angle of incidence.

Results of a water surface scan are illustrated in Figure 4, along with predicted brightnesses based on numerical radiative transfer calculations (see also Appendix B). The transformed feedhorn brightnesses track the predicted values well, as indicated by the nearly-constant values of T_V, T_H, and U. Ideally, these would remain constant throughout the scan. However, a small systematic error of less than 7 K was caused by mechanical misalignment of the scan mirror and feedhorn axes. In practice, precise alignment would eliminate this error. Other sources of discrepancy between the predicted and measured brightnesses include errors in the assumed atmospheric state, which was taken to be the US standard atmosphere for the purpose of this comparison.

D. Alternatives

As an alternative to EPBR and the associated calibration scheme, another means of achieving electronic rotation of two orthogonal-linear feedhorn modes was considered. This technique uses ferromagnetic devices based on the Faraday effect. These devices can provide selectable rotation of orthog
onally-polarized circular waveguide modes in response to the strength of an applied DC magnetic field. However, they have the following shortcomings for radiometric applications:

* The bandwidths are inherently small (1%). At least 2 GHz bandwidths are desirable for radiometric observations near 90 GHz.

* They are somewhat lossy (>1 dB at 90 GHz), and hence reduce

radiometer sensitivity.

* Practical Faraday rotators are currently unavailable for frequencies above 100 GHz. (Future passive microwave observations of cirrus observations may require polarized observations at frequencies as high as 340 GHz.)

* At best, Faraday rotators can be used only over a single radiometric band. This precludes their use in multiband feed systems, such as SSM/I or TMI.

The EPBR technique overcomes all these limitations with minimal hardware complexity and the added capability to observe both the third and fourth Stokes parameters U and V.

E. Radiative Transfer Model

Most of our efforts during the period of this grant have focussed on the construction of hardware for the ground-based demonstration instrument. However, some progress was made in upgrading the Georgia Tech MRT numerical radiative transfer model. This code, the original version of which was written by the author at the Massachusetts Institute of Technology in 1987, is a comprehensive scattering-based numerical radiative transfer model. Currently, the model incorporates scattering and absorption from liquid and frozen spherical hydrometeors. In order to interpret polarized microwave brightness temperatures observed over precipitation, the model is being upgraded to accommodate aspherical liquid and ice particles.

The MRT numerical model uses an iterative (or perturbation) approach to calculate the temperature weighting functions for a planar-stratified scattering and absorbing atmosphere. Hydrometeors are currently modelled by Marshall-Palmer distributed liquid spheres and Sekhon-Srivastava distributed ice spheres. To be useful in interpreting polarized microwave brightness temperatures caused by aspherical hydrometeors, modifications to the phase matrix, extinction matrix and absorption vector computation are required. Development of subroutines to calculate these quantities for

planar-stratified distributions of prolate and oblate spheroidal hydrometeors is ongoing.

For electrically small particles, the Rayleigh-Gans approximation will be used. For electrically large particles, an exact solution using spheroidal coordinates for the scattered field of a single spheroidal particle (Asano and Sato, 1980) was investigated. However, two attributes make this approach undesirable: (1) lack of reliable routines for calculating the vector spheroidal wave functions required by this formulation, and (2) the number of nested summations required. The T-matrix approach (Tsang, et al, 1985) is more desirable because the formulation is based on the more familiar vector spherical modes, and the number of nested summations will be fewer.

A major problem in aspherical hydrometeor radiative transfer modelling is determining realistic models of ice hydrometeor particle size, shape, and orientation distributions, particularly within cirrus anvils and thunderstorm tops. To this end, we are investigating a statistical relationship between aspherical particle orientation and the local atmospheric electric field. In order to minimize electrostatic energy, particles will preferentially align themselves with their longest axis in the direction of the field (Stratton, 1941). The resulting canting angle distribution can be computed using a Boltzman probability distribution.

The relationship between the local field and particle orientation has been hypothesized to be the cause of observed changes in the phase delay and depolarization of microwave signals received from satellite beacons (Cox and Arnold, 1979). It is also plausible that polarized microwave brightness temperatures could be used to identify regions of atmospheric electrification, or vice-versa.

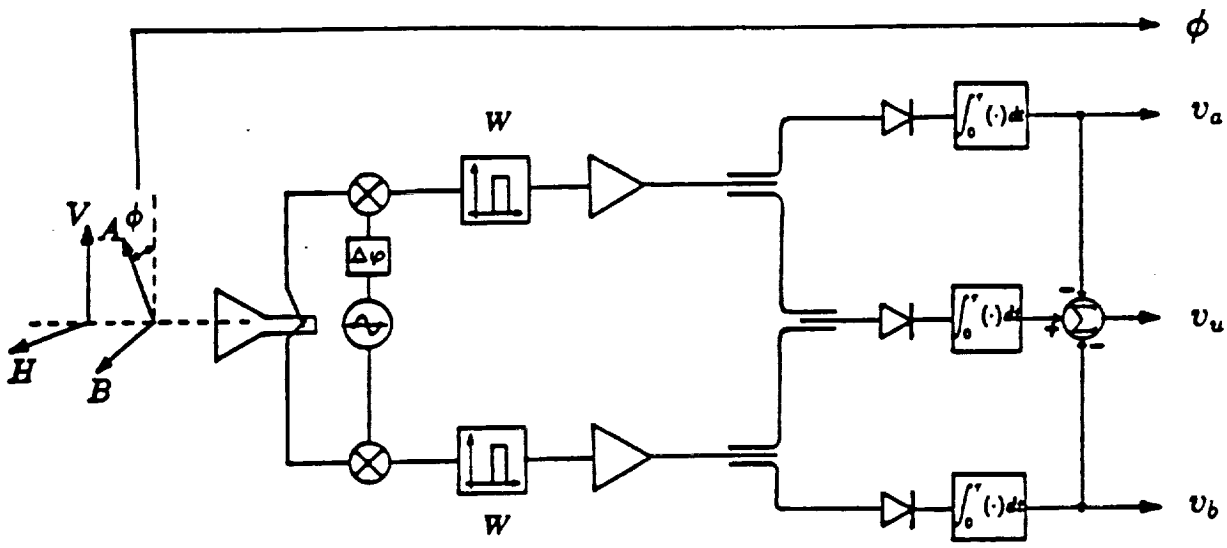

Figure 1. Block diagram of the three-channel (T_A, T_U, and T_B) radiometer used to implement electronic polarization basis rotation.

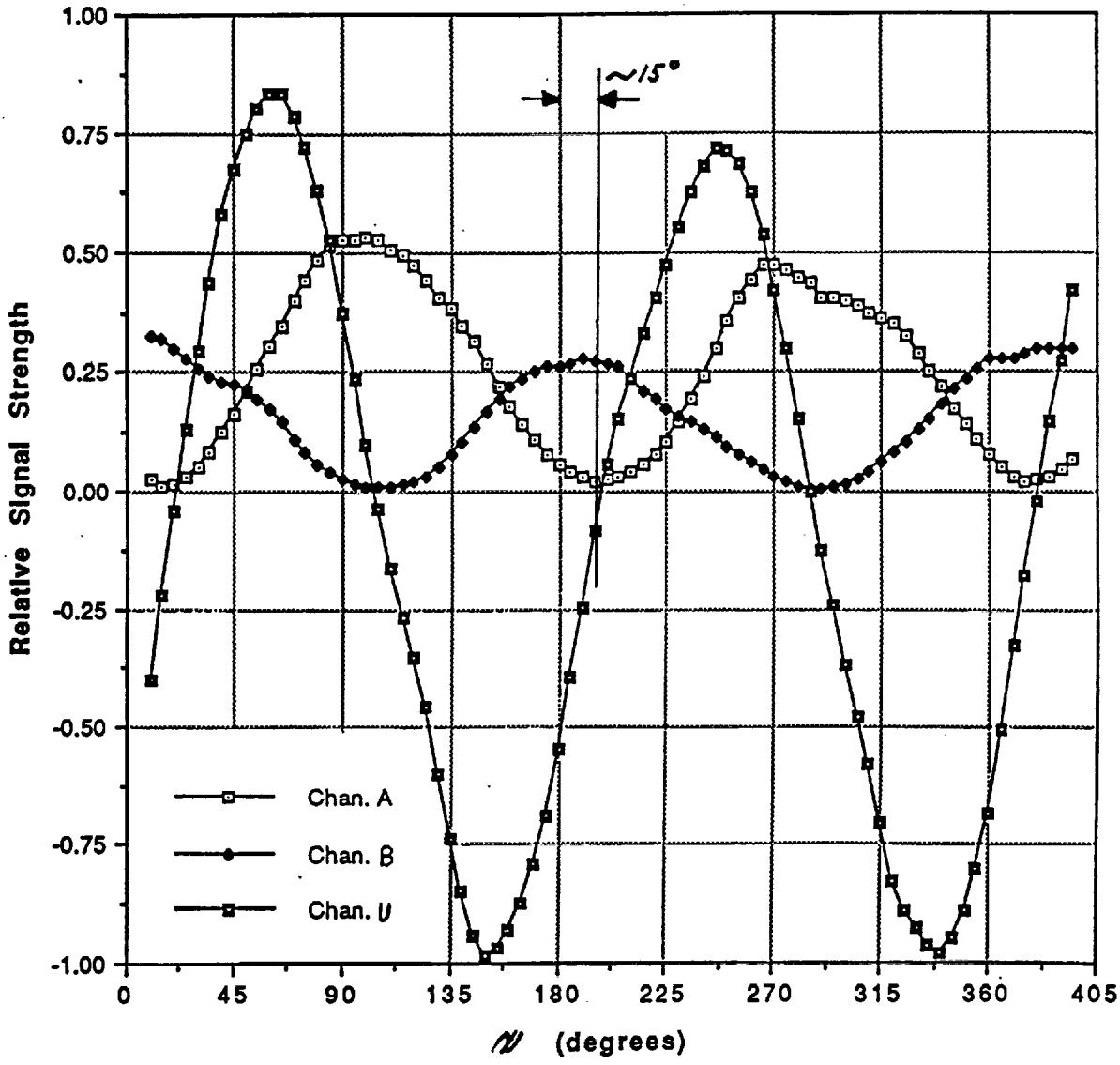

Figure 2. Responses of auto- and cross-correlation channels to a 90-GHz CW source as a function of the polarization angle ψ of the source.

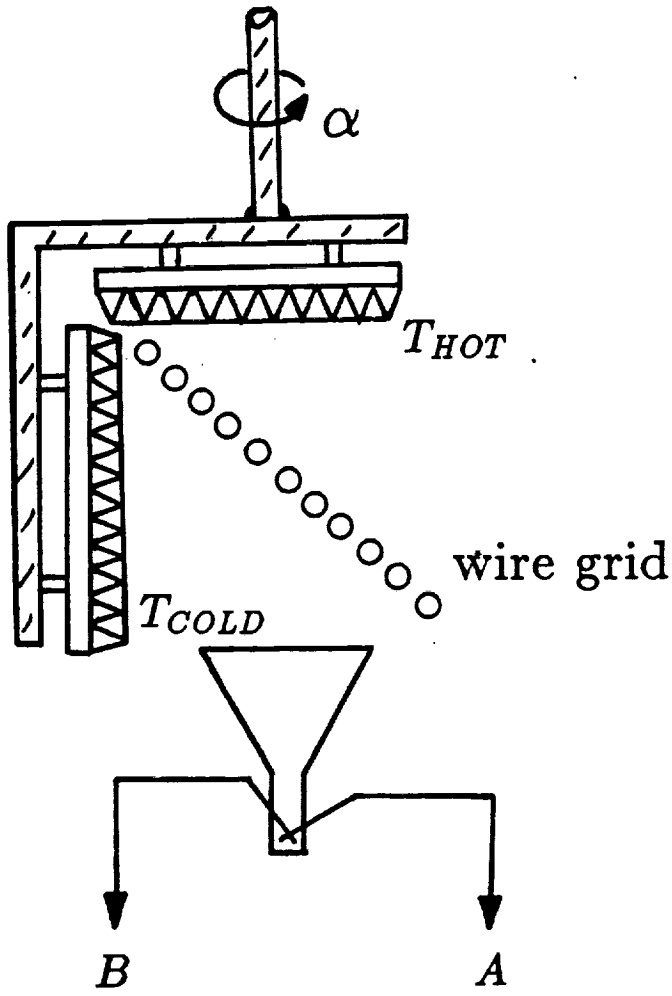

Figure 3. Schematic of the polarized load used to calibrate the cross-correlating radiometer.

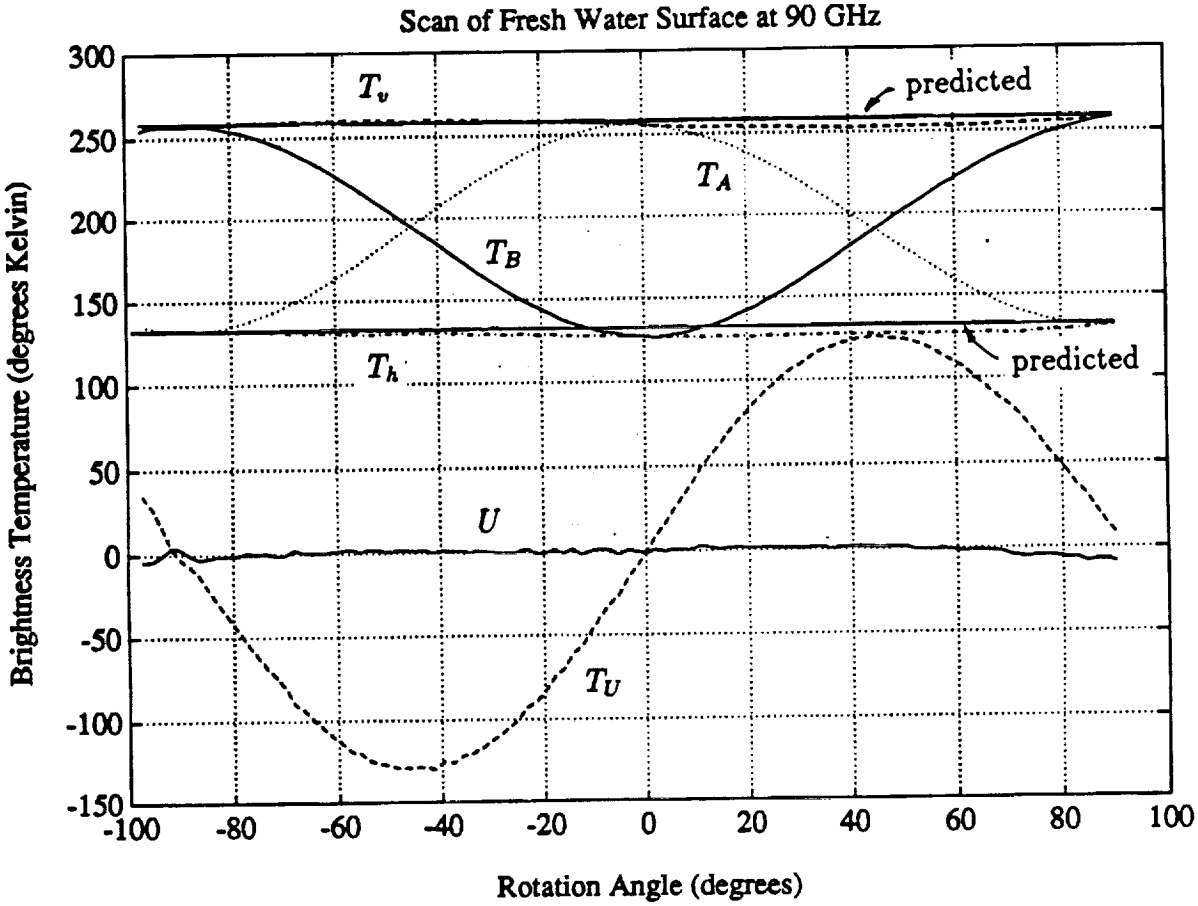

Figure 4. Results of near-Brewster angle conical scans of a highly polarizing water surface. The parameters T_A, T_U, and T_B are the measured feedhorn brightnesses; T_V, T_H, and U are the resulting transformed brightnesses in the Earth's vertical-horizontal basis. The brightnesses predicted using a numerical radiative transfer model are illustrated by the heavy lines.

CONCLUSIONS AND RECOMMENDATIONS

The results of the calibration experiments and water scans effectively demonstrate that EPBR is a practical alternative to mechanical rotation of a dual-polarization radiometer about its feedhorn axis. Applications of the technique include both conical and cross-track scanning instruments, although the cross-track scanner benefits less since polarization information is typically not useful at observation angles less than 30^{o} from nadir. For an instrument designed to measure all four Stokes parameters, the EPBR technique has a decided advantage, since switching between measurements of U and V requires only a single LO phase shift.

Our recommendations with respect to EPBR and its applications are fourfold:

(1) It would be interesting to commence ground-based observations of polarized microwave emissions from precipitation cells. Such observations could be used to investigate correlations between oriented ice particles and thunderstorm electrification. To support this investigation, a two-axis imaging scanhead is being planned for use with the 90-GHz ground-based radiometer. To complement the passive measurements, coincident downlink scintillation and depolarization measurements using a satellite beacon (e.g., ACTS) are being considered. The local electric field strength can be measured using an electric field mill probe. The results of coincident passive, active and electric field measurements could provide an improved understanding of propagation through regions of oriented ice particles, particularly thunderstorm anvils.

(2) To provide polarized high resolution images of precipitation cells as would be observed from a satellite, the implementation of an aircraft-based imaging radiometer with EPBR is recommended. Two practical options might be considered. The first is a modification of the Advanced Microwave Precipitation Radiometer (AMPR) to include EPBR. (A proposal describing suggested EPBR modifications has recently been submitted by the authors of

this report to the contract monitor at NASA/MSFC.) This would be a relatively inexpensive means of achieving broadband dual-polarization imaging capability, but suffers from two non-critical problems. First, the mechanics of retrofitting the AMPR with suitable polarized and unpolarized loads will be difficult due to the space restrictions. Second, the resulting cross-track scanned images would exhibit useful polarization information only near the ends of the scan.

A second option (albeit more expensive) is to construct a new conically-scanned instrument based on EPBR for flights on either the NASA DC-8 or ER-2. Suggested frequencies include window channels at 18, 37, 90, 155, 220, and 340 GHz. The instrument would be particularly useful for studying polarized emissions from electrified thunderstorm anvils and thin clouds over water backgrounds. By virtue of its conical-scan imaging mode, such an instrument could also provide accurate underflight data for the SSM/I, TMI, and MIMR instruments.

(3) Measurement and interpretation of the full Stokes vector over a wave-covered water surface at oblique viewing angles will provide information needed to optimize remote sensing techniques for ocean surface winds. Under appropriate conditions, it has been shown to be possible to remotely sense the direction of propagating gravity or capillary waves on the water surface, thereby providing a measurement of surface wind direction (Wentz, 1991).

To further investigate the potential ability of a satellite-based conically-scanned radiometer to remotely sense ocean surface wind direction, we recommend measurements using the 90-GHz ground-based instrument observing a simulated wave-covered ocean surface. Thus, the sensitivity of the Stokes' parameters T_V, T_H and V to wave direction can be investigated. All of these parameters can be measured simultaneously using the 90-GHz ground-based radiometer provided that the LO phase at one of the two mixers is shifted by 90^o. This can currently be done manually. Simulated ocean wave models of various heights and periods can be constructed from a low-loss, low-dielectric constant matrix (e.g., open-

cell foam) saturated and covered with oceanic saline. In this manner, the emissivity of an ocean wave in the geometric optics limit can be studied in detail as a function of observation angle.

A means for electronically (as opposed to manually) shifting the LO phase in order to facilitate fast, reliable switching of a spaceborne EPBR radiometer from the U measurement mode to the V mode should also be demonstrated. This can be accomplished using ferrite switched circulators.

(4) In order to interpret aircraft- and ground-based thunderstorm and simulated ocean wave observations, it is recommended to continue the polarized radiative transfer modelling commenced during this grant. This modelling emphasis has two components: (A) millimeter-wave radiative transfer modelling within oriented needle- and plate-shaped ice crystals using an ellipsoidal particle model, and (B) reflectivity and emissivity modelling of lossy periodic surfaces, in particular, capillary and gravity ocean surface waves, viewed at oblique angles.

Our specific recommendation is to upgrade the Georgia Tech MRT numerical code. The overall goal will be to use the model to interpret the experimental data, and to develop passive microwave retrieval algorithms for cloud and precipitation parameters, and ocean surface wind direction. Aspherical RT calculations will be essential in developing precipitation parameter retrieval methods using polarized microwave observations, and interpreting both airborne and ground-based polarized microwave observations. We also recommend investigation of the hypothesized relationship between polarized microwave brightness temperatures caused by frozen hydrometeors and the local atmospheric electric field. An additional useful capability would be full Stokes vector calculations (i.e., all four parameters) over a wave-covered ocean surface. This upgrade will be critical in investigating the ocean surface wind-direction sensing capabilities of full-polarization passive microwave brightness measurements.

REFERENCES

Asano, S., and M. Sato, "Light Scattering by Randomly Oriented Spheroidal Particles", Appl. Opt., 19, 6, 962-974, 1980.

Cox, D.C. and H.W. Arnold, "Observations of Rapid Changes in the Orientation and Degree of Alignment of Ice Particles Along an Earth-Space Radio Propagation Path", J. Geophys. Res., 84, C8, 5003-5010, 1979.

Gasiewski, A.J., and D.H. Staelin, "Numerical Analysis of Passive Microwave O_2 Observations Over Precipitation", Radio Science, 25, 3, 217-235, 1990.

Gasiewski, A.J., "A Technique for Measuring Vertically and Horizontally Polarized Microwave Brightness Temperatures Using Electronic Polarization-Basis Rotation", Proceedings of the 1990 International Geoscience and Remote Sensing Symposium, 1569-1572, University of Maryland, College Park, MD, May 20-24, 1990.

Parks, G.S., T.C. Fraschetti, and D.C. Miller, Microwave Precipitation Radiometer, Jet Propulsion Laboratory Study Report JPL D-5397, May 1, 1988.

Stratton, J.A., Electromagnetic Theory, New York: McGraw-Hill, 1941.

Tsang, L., J.A. Kong, and R.T. Shin, Theory of Microwave Remote Sensing, New York: John Wiley and Sons, 1985.

Wentz, F., "Measurement of Oceanic Wind Vector Using Satellite Microwave Radiometers", RSS technical report 051591, Remote Sensing Systems, Inc., May 15, 1991.

APPENDIX A

(Proceedings of the 1990 International Geoscience and Remote Sensing Symposium, pp. 1569-1572, University of Maryland, College Park, MD, May 20-24, 1990.)

A Technique for Measuring Vertically and Horizontally Polarized Microwave Brightness Temperatures Using Electronic Polarization-Basis Rotation

A.J. Gasiewski

School of Electrical Engineering
Georgia Institute of Technology, Atlanta, GA 30332-0250

Abstract-A combined hardware and software technique is described for the measurement of the vertically and horizontally polarized components of the atmospheric microwave brightness temperature at arbitrary scan angles using a fixed-feed dual-polarization conical or cross-track scanner. The technique is an implementation of electronic polarization basis rotation, and is facilitated by the correlation of the in-phase amplitudes of two orthogonal linearly-polarized feedhorn modes. A linear minimum mean-square-error estimator is subsequently used to infer the vertical and horizontal brightnesses from the radiometer outputs. A practical hardware configuration and calibration scheme is presented.

The technique is particularly useful for passive microwave precipitation parameter retrieval using spaceborne or airborne conical scanners. The ultimate performance of the technique depends on the calibration of the receiver and balancing of the radiometer channels. Laboratory and aircraft flight tests of electronic polarization basis rotation are planned.

Key Words- radiometer, polarization, microwave, precipitation.

1. Introduction

Recent investigations into passive microwave remote sensing of precipitation have suggested that the difference between the vertically and horizontally polarized brightness temperatures contain useful information concerning the intensity of precipitation over ocean [1,2], and possibly, the presence of aspherical particles in the cell top [3]. The polarization difference can also be used as an aid in detecting snow cover and discriminating between land and water backgrounds [4].

For the terrestrial troposphere and lower stratosphere, and for frequencies at which non-reciprocal propagation effects caused by the Earth's magnetic field can be neglected, only the vertical and horizontal Stokes' parameter brightness temperatures (T_V and T_H) are non-zero. Hence, it is appropriate to design earth-probing instruments to measure, at most, these two parameters. Because the $V-H$ polarization basis requires a miminal number of non-zero parameters (2) to uniquely describe the radiation field, it is termed the "natural" polarization basis.

2. Measurement of T_V and T_H

Ideally, the polarization basis of an airborne or spaceborne dual linearly-polarized radiometer should coincide with the natural polarization basis, so that the two radiometer channel outputs will be (upon proper calibration) T_V and T_H. Unfortunately, the need to image extended regions of the atmosphere by physically scanning the antenna beam makes it difficult to build an instrument which retains polarization coincidence with the natural basis at every spot. Consider two common scanner configurations for passive microwave imaging: conical and cross-track. The conical scanner is typically consists of an off-axis parabolic antenna rotating about the feedhorn axis, thus sweeping the antenna beam through a cone-shaped swath. The cross-track scanner consists of a rotating scan mirror oriented 45° with respect to the feedhorn axis. The resulting wedge- shaped swath is typically oriented transverse to the motion of the platform, yielding a raster scan below the flight track.

In their simplest configurations, both conical and cross-track scanners employ a feedhorn fixed rigidly to the instrument platform. For dual linearly-polarized feedhorns, this results in the feedhorn polarization basis rotating (with respect to the natural basis) during the scan. The angular difference ϕ between the two bases is termed polarization basis skew (the two bases coincide at $\phi = 0$). To obtain zero polarization skew at all scan angles, the feedhorn might be mechanically rotated along with the scanning reflector. However, alignment of the feedhorn and natural polarization bases by mechanical rotation is both cumbersome and expensive.

As suggested by Parks *et al.* [5] for the conical scanner, a more desireable way to eliminate the polarization skew throughout the scan is to employ an inexpensive fixed-feed scanner, and to electronically rotate the polarization basis. The linear transformation of brightness temperatures $\overline{T}$ from the natural polarization basis to feedhorn temperatures $\overline{T}_f$ in the instrument's polarization basis is:

$$\begin{pmatrix} T_{fA} \\ T_{fB} \\ T_{fU} \end{pmatrix} = \begin{bmatrix} \cos^2\phi & \sin^2\phi & \frac{1}{2}\sin 2\phi \\ \sin^2\phi & \cos^2\phi & -\frac{1}{2}\sin 2\phi \\ -\sin 2\phi & \sin 2\phi & \cos 2\phi \end{bmatrix} \begin{pmatrix} T_V \\ T_H \\ T_U \end{pmatrix}$$

$$= \overline{U}(\phi)\cdot\overline{T} \qquad (1)$$

where $T_{fU} = Re\langle E_A E_B^* \rangle$ is the cross-correlation between the two orthogonal linearly polarized feedhorn modes (A and B), and ϕ is related to the scan angle. In practice, the measured value of

$\overline{T}_f$ (denoted $\hat{\overline{T}}_f$) is corrupted by additive instrument noise due to calbration errors and finite integration time:

$$\hat{\overline{T}}_f = \overline{U}(\phi) \cdot \overline{T} + \overline{n}_T \qquad (2)$$

With electronic polarization basis rotation, the brightness temperatures in the natural basis are estimated using the measured brightnesses in the feedhorn basis. The estimation of T_V and T_H are facilitated by the measurement of T_{fU} along with T_{fA} and T_{fB}. We address three issues concerning the practical implementation of electronic polarization basis rotation on both cross-track and conical scanners: 1) the hardware configuration of a T_{fU}-channel exhibiting acceptably small crosstalk and instrument noise. 2) calibration of the T_{fU}-channel, 3) an algorithm for estimating the brightness vector $\overline{T}$ in the natural basis from the measured data $\hat{\overline{T}}_f$ in the feedhorn basis.

3. Hardware

Fig. 1 illustrates a practical configuration of microwave and analog hardware for the measurement of the three components of $\overline{T}_f$. The radiometer consists of a single superheterodyne down-conversion stage for each of two channels A and B, and a cross-correlating channel U. The phase shift $\Delta\phi$ is adjusted to cancel any RF path-length differences between the A and B channels. Square-law detectors and integrators provide voltage outputs proportional to the signal power in the respective intermediate frequency (IF) channels.

To implement the U-channel, the A and B IF signals are added prior to detection. The output voltage vector $\overline{v}$ is thus related to the feedhorn temperatures by:

$$\begin{pmatrix} v_A \\ v_B \\ v_U \end{pmatrix} = \begin{bmatrix} g_{AA} & 0 & 0 \\ 0 & g_{BB} & 0 \\ g_{AU} & g_{BU} & g_{UU} \end{bmatrix} \cdot \begin{pmatrix} T_{fA} \\ T_{fB} \\ T_{fU} \end{pmatrix} + \begin{pmatrix} o_A \\ o_B \\ o_U \end{pmatrix} + \overline{n}_v$$

$$= \overline{\overline{g}}\,\overline{T}_f + \overline{o} + \overline{n}_v \qquad (3)$$

where $\overline{\overline{g}}$ and $\overline{o}$ are instrument gain and offset parameters, respectively, and $\overline{n}_v = \overline{\overline{g}}\,\overline{n}_T$ is the instrument noise referred to the video outputs. Upon calibration, the feedhorn brightness temperatures are subsequently found from the output voltages:

$$\hat{\overline{T}}_f = \overline{\overline{g}}^{-1}(\overline{v} - \overline{o}) \qquad (4)$$

In order to detect the relatively small cross-correlation signal T_{fU} in the presence of the larger signals T_{fA} and T_{fB}, the video outputs of the A and B channels are subtracted from the U-channel video output. Provided that the total IF and video gains associated with the power splitters, square-law detectors, and integrators are matched to within ~ 0.5 dB, the gain parameters g_{AU} and g_{BU} will be small compared to g_{UU} (thus minimizing crosstalk), and the instrument noise $\overline{n}_T$ will be nearly white, with covariance:

$$\overline{\overline{R}}_{n_T n_T} = \langle \overline{n}_T \overline{n}_T^t \rangle \approx \sigma_T^2 \overline{\overline{I}} \qquad (5)$$

where $\overline{\overline{I}}$ is the identity matrix, and $(\cdot)^t$ is the transpose operator. The noise standard deviation is:

$$\sigma_T = \frac{T_{SYS}}{\sqrt{W\tau}} \qquad (6)$$

where T_{SYS} is the system noise temperature (receiver plus antenna), W is the IF bandwidth, and τ is the effective integration time. In practice, balancing is accomplished by video and IF component matching and thermal stabilization.

4. Calibration

Calibration of all channels can be accomplished using a polarised calibration device (Fig. 2) consisting of two highly-absorbing microwave blackbody loads and a polarisation-splitting wire grid. One load is cooled to a low kinetic temperature T_{COLD}, and the other heated to a high temperature T_{HOT}, where $T_{HOT} - T_{COLD} \approx 80$ K. The wire grid combines the two load brightness temperatures into two orthogonal- linear polarizations. Each brightness temperature is precisely calculable from thermcouple or thermistor measurements of T_{HOT} and T_{COLD}, along with a-priori knowledge of the wire grid transmission and reflection coefficients [6], the load emission and bistatic scattering properties, and the load background brightness temperatures.

By rotating the device about the feedhorn axis, the radiometer feed can be illuminated by a set of known, linearly independent brightness temperature vectors. In practice, observations would be made at four values of the load angle α: 0°, 45°, 90°, and 135°. The four U-channel observations are related to the load temperatures by:

$$\begin{pmatrix} v_U(\alpha = 0^\circ) \\ v_U(\alpha = 45^\circ) \\ v_U(\alpha = 90^\circ) \\ v_U(\alpha = 135^\circ) \end{pmatrix} = \overline{n}_v +$$

$$\begin{bmatrix} T_{HOT} & T_{COLD} & 0 & 1 \\ \frac{T_{HOT}+T_{COLD}}{2} & \frac{T_{HOT}+T_{COLD}}{2} & \frac{T_{HOT}-T_{COLD}}{2} & 1 \\ T_{COLD} & T_{HOT} & 0 & 1 \\ \frac{T_{HOT}+T_{COLD}}{2} & \frac{T_{HOT}+T_{COLD}}{2} & \frac{T_{COLD}-T_{HOT}}{2} & 1 \end{bmatrix} \cdot \begin{pmatrix} g_{UA} \\ g_{UB} \\ g_{UU} \\ o_U \end{pmatrix} \qquad (7)$$

5. Expected Performance

A linear estimator is used to infer $\overline{T}$ from the noisy measurements $\hat{\overline{T}}_f$:

$$\hat{\overline{T}} = \overline{\overline{D}}(\phi) \cdot (\hat{\overline{T}}_f - \langle \hat{\overline{T}}_f \rangle) + \langle \overline{T} \rangle \qquad (8)$$

where $\langle \cdot \rangle$ is the statistical mean. Using a minimum mean-square-error (MMSE) criterion, the optimum LMMSE estimator is:

$$\overline{\overline{D}} = \overline{\overline{R}}_{TT} \overline{\overline{U}}^t \left[\overline{\overline{U}}\,\overline{\overline{R}}_{TT}\,\overline{\overline{U}}^t + \overline{\overline{R}}_{n_T n_T} \right]^{-1} \qquad (9)$$

where $\overline{\overline{R}}_{TT}$ is the covariance matrix for the brightness vector in the natural basis. The measurement error covariance matrix becomes:

$$\overline{\overline{R}}_{EE} \equiv \langle (\hat{\overline{T}} - \overline{T})(\hat{\overline{T}} - \overline{T})^t \rangle$$
$$= (\overline{\overline{I}} - \overline{\overline{D}}\,\overline{\overline{U}}) \overline{\overline{R}}_{TT} (\overline{\overline{I}} - \overline{\overline{D}}\,\overline{\overline{U}})^t + \overline{\overline{D}}\,\overline{\overline{R}}_{n_T n_T} \overline{\overline{D}}^t \qquad (10)$$

Fig. 3 shows LMMSE calculations of the expected errors in $\hat{T}_V$, $\hat{T}_H$, and $\hat{T}_{V-H} \equiv \hat{T}_V - \hat{T}_H$ as a function of ϕ for a typical conical scanner. The calculations assume $\sigma_T = 1$ K, a standard deviation of 50 K for the vertical and horizontal brightness temperatures, and a standard deviation of 7 K for the vertical-horizontal brightness difference $T_{V-H} \equiv T_V - T_H$:

$$\overline{\overline{R}}_{TT} = \begin{bmatrix} 2500 & 2475.5 & 0 \\ 2475.5 & 2500 & 0 \\ 0 & 0 & 0 \end{bmatrix} \qquad (11)$$

These statistics are expected for conical swaths with $\sim 45°$ half-cone angles [2]. The vertical and horizontal electric fields are assumed to be uncorrelated ($T_U = 0$), which is equivalent to the assumption that the $V - H$ basis is the natural basis.

Calculations of the expected measurement error using the LMMSE estimator were performed for fixed-feed dual-polarization radiometers configured both with ("3-parameter") and without ("2-parameter") the U-channel (Fig. 3). The electronic polarization basis rotation technique suggests significantly smaller measurement errors in $\hat{T}_V$, $\hat{T}_H$, and the difference $\hat{T}_{V-H}$ than possible using a fixed-feed dual-polarized radiometer without the U-channel. The improvement is particularly striking for polarization skew angles near 45°. With the electronic technique, the measurement error is practically independent of ϕ, and hence, independent of the scan position within the conical swath.

For a cross-track scanner, the antenna beam is oriented over a range of observation angles (typically from nadir+45° to nadir-45°) during the scan. Near nadir, the brightness difference T_{V-H} drops to zero, (i.e., T_V and T_H become indistinguishable). The correlation between T_V and T_H as a function of observation angle θ (measured with respect to nadir) can be modelled approximately by:

$$R_{T_V T_H} = 2475.5 + 24.5\cos(2\phi) \qquad (12)$$

This relationship has been incorporated into the LMMSE estimator. Assuming that the nadiral scanner spot has a polarization skew angle $\phi = 45°$, smaller measurement errors in $\hat{T}_{V-H}$ result near $\phi = 45°$ than in the case of the conical scanner (Fig. 4, "3-parameter"). However, since the nadiral $T_V - T_H$ correlation can also be exploited using a conventional dual-polarized radiometer (with no U-channel) and a LMMSE estimator (Fig. 4, "2-parameter"), a smaller reduction in error is realized by the addition of the U-channel to a cross-track scanner than when added to a conical scanner.

6. Discussion

Because of potential applications in conical and cross-track scanning microwave precipitation radiometers, we plan to prove the concept of electronic polarization rotation through both laboratory and aircraft experiments. Our laboratory test will use the NASA Goddard Space Flight Center's 92-GHz dual-polarized fixed-beam radiometer. Overall performance will be judged using Brewster-angle observations of a water surface, which exhibits strong, predictable microwave polarization characteristics. Pending favorable laboratory results, we have proposed to implement the technique on the 85-GHz channel of the NASA Marshall Space Flight Center's Advanced Microwave Precipitation Radiometer (AMPR). The AMPR is a cross-track microwave scanner configured for operation on board the NASA ER-2 high-altitude aircraft with channels at 10, 19, 37, and 85 GHz. Although the error reduction attainable using electronic polarization basis rotation on a cross-track scanner is not as large as that attainable on a conical scanner, it is nonetheless large enough to be useful.

Acknowledgements-This work has been supported by the Georgia Institute of Technology.

References

[1] Spencer, R.W., A Satellite Passive 37-GHz Scattering-based Method for Measuring Oceanic Rain Rates, *J. Cli. Appl. Meteor.*, Vol. 25, No. 6, pp. 754-766, 1986.

[2] Adler, R.F., R.A. Mack, N. Prasad, H.-Y.M. Yeh, and I.M. Hakkarinen, Aircraft Microwave Observations and Simulations of Deep Convection from 18-183 GHz Part I: Observations, Accepted for publication in *J. Ocean Atm. Tech.*, 1989.

[3] Kummerow, C.D., and J.A. Weinman, Radiative Properties of Deformed Hydrometeors for Commonly Used Passive Microwave Frequencies, *IEEE Trans. Geosci. Remote Sensing*, Vol. GE-26, No. 5, pp. 629-637, 1988.

[4] Negri, A.J., R.F. Adler, and C.D. Kummerow, False-Color Display of Special Sensor Microwave/Imager (SSM/I) Data, *Bull. Am. Meteor. Soc.*, Vol. 70, No. 2, pp. 146-151, 1989.

[5] Parks, G.S., T.C. Praschetti, D.C. Miller, *Microwave Precipitation Radiometer*, Jet Propulsion Laboratory Study Report JPL D-5397, May 1, 1988.

[6] Chambers, W.G., T.J. Parker, and A.E. Costley, Free-standing Fine-Wire Grids for Use in Millimeter- and Submillimeter-Wave Spectroscopy, in *Infrared and Millimeter Waves*, K.J. Button (ed.), Vol. 16, pp. 77-106, 1986.

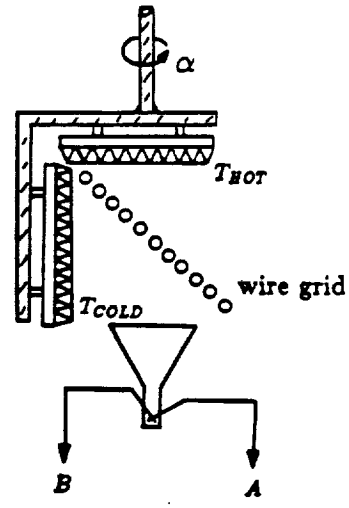

Figure 2: Proposed dual-polarized calibration load for use with the 3- channel radiometer. The angle α is variable, thus producing a set of known brightness vectors (T_{fA}, T_{fU}, T_{fB}).

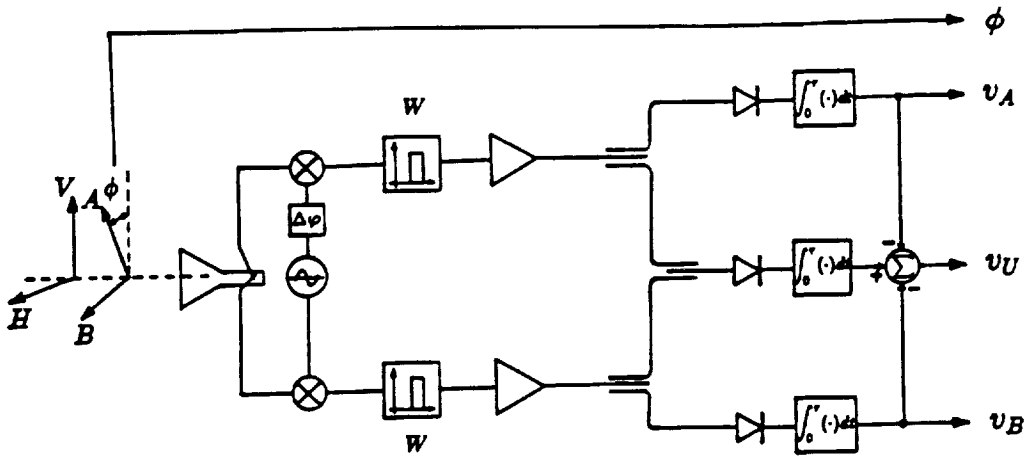

Figure 1: Block diagram of a practical 3-channel (T_{fA}, T_{fB}, and T_{fU}) radiometer to implement electronic polarization basis rotation.

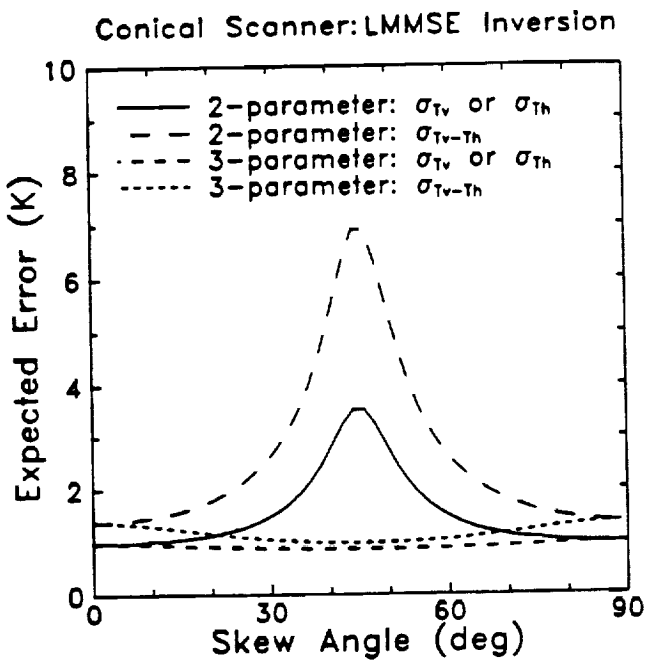

Figure 3: Comparison of expected errors for a conical scanner employing LMMSE polarization basis rotation without (2-parameter) and with (3- parameter) information from the U-channel. Error estimate curves are shown for measurements of T_V (or equivalently, T_H) and $T_V - T_H$.

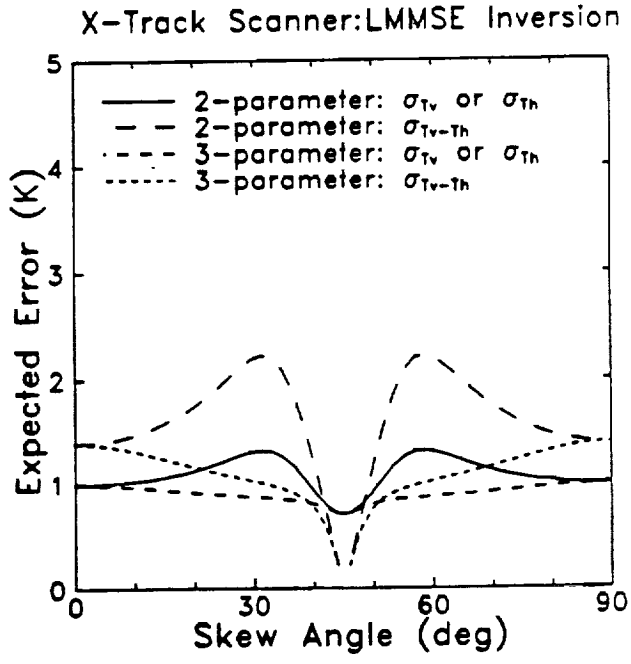

Figure 4: Comparison of expected errors for a cross-track scanner employing LMMSE polarization basis rotation without (2-parameter) and with (3-parameter) information from the U-channel. Error estimates are shown for measurements of T_V (or equivalently, T_H) and $T_V - T_H$. The LMMSE estimator uses the correlation between T_V and T_H at scan angles near nadir (i.e., skew angles near 45°).

APPENDIX B

(Submitted to the 1992 International Conference on Microwave Symposium, Albequerque, NM, June 1-5, 1992.)

Laboratory Demonstration of
Electronic Polarization Basis Rotation

A.J. Gasiewski, D.B. Kunkee
School of Electrical Engineering
Georgia Institute of Technology
Atlanta GA, 30332-0250

Summary

In microwave Earth remote sensing, it is often desirable to build passive imaging radiometers with dual orthogonal-linear polarization sensitivity. The additional information obtained by observing both vertically and horizontally polarized brightness temperatures can be used to improve estimates of rainfall, water vapor, and ocean surface winds, and to enhance the detectability of sea ice. However, in order to retain coincidence between the radiometer feedhorn's polarization basis and the Earth's vertical-horizontal basis, previous mechanically-scanned imager designs have required that the feedhorn and associated receiver electronics be physically rotated along with the scanning mirror. This is both cumbersome and expensive.

By measuring the first three feedhorn Stokes parameters (T_A, T_B, and T_U), the measured Stokes vector can be transformed into any desired basis, including the natural basis defined by the local vertical and horizontal directions. The technique is called "Electronic Polarization Basis Rotation" [1]. A practical implementation of EBPR was proposed by Gasiewski [2], whose scheme included a polarized calibration load. In this article, we report the first successful demonstration of a well-calibrated polarization correlation radiometer with EBPR capabilities.

The radiometer (depicted schematically in Figure 1) is a 90-GHz dual orthogonal linear polarization unit with three outputs: one for each of the two orthogonal polarizations (v_a and v_b) and a cross-correlation channel (v_u). The v_u channel is formed by an adding correlator with the addition of a post-detection summing circuit. This circuit removes the relatively large signals caused by the squaring of the IF voltages in each of the channels A and B. The result is three signals that are linearly related to the first three feedhorn Stokes' parameters:

$$\overline{v} = \overline{\overline{g}} \begin{bmatrix} T_A \\ T_U \\ T_B \end{bmatrix} + \overline{o} + \overline{n} \qquad (1)$$

where $\overline{v}$ represents the three video output signals from the radiometer depicted in Figure 1, $\overline{\overline{g}}$ and $\overline{o}$ are the instrument gain and offset pa-

rameters, and $\overline{n}$ is the instrument noise referred to the video outputs. Dicke-switching is used to reduce the effects of receiver gain and offset fluctuations. The phase difference of the local oscillator signal at each mixer was nulled using a phase shift $\Delta\varphi$. In addition the path length of the two IF signals was equalized to well within a correlation length $l_c \sim v_p/W$, where v_p is the phase velocity, and W is the bandwidth (Figure 1).

The parameters $\overline{\overline{g}}$ and $\overline{o}$ are needed to convert the measured voltage data into feedhorn brightnesses. However, both $\overline{\overline{g}}$ and $\overline{o}$ remain stable only over a time scale of minutes, and thus need to be periodically estimated. Moreover, interchannel crosstalk (indicated by nonzero diagonal elements in $\overline{\overline{g}}$) occurs. For example, imperfect adjustment of the summing circuit causes the off-diagonal elements in the second row of $\overline{\overline{g}}$ to be nonzero. Similarly, polarization crosstalk causes the off-diagonal elements in the first and third rows of $\overline{\overline{g}}$ to be nonzero. The measured cross polarization rejection was approximately 15 dB.

A calibration procedure employing a unique polarized calibration load (Figure 2) was successfully used to estimate all elements in $\overline{\overline{g}}$ and $\overline{o}$. The procedure requires an observation of the calibration load assembly at three unique values of α in addition to an observation of a non-polarized load. Four different observations (each resulting in 3 measured values) are required to achieve an observation matrix of full rank enabling estimation of all twelve elements in $\overline{\overline{g}}$ and $\overline{o}$.

Once $\overline{\overline{g}}$ and $\overline{o}$ have been determined, the feedhorn brightness temperatures ($\overline{T}_f$) can be estimated from the video outputs,

$$\hat{\overline{T}}_f = \begin{bmatrix} T_A \\ T_U \\ T_B \end{bmatrix} = \overline{\overline{g}}^{-1}(\overline{v} - \overline{o}) \tag{2}$$

The value of $\hat{\overline{T}}_f$ is then used to estimate $\overline{T}$, the three Stokes parameters in the Earth's vertical-horizontal basis [1]:

$$\hat{\overline{T}} = \begin{bmatrix} T_v \\ U \\ T_h \end{bmatrix} = \begin{bmatrix} \cos^2(\phi) & -\frac{1}{2}\sin(2\phi) & \sin^2(\phi) \\ \sin(2\phi) & \cos(2\phi) & -\sin(2\phi) \\ \sin^2(\phi) & \frac{1}{2}\sin(2\phi) & \cos^2(\phi) \end{bmatrix} \hat{\overline{T}}_f \tag{3}$$

where ϕ is the polarization skew angle as shown in Figure 1.

Near Brewster-angle observations of a water surface using a conically scanned mirror demonstrate the ability to rotate the polarization

basis, that is to obtain $\hat{\overline{T}}$ from $\hat{\overline{T}}_f$. A conical scan was performed with an observation angle of 65° with respect to vertical (nadir) at a height of a few feet over the water surface. To continuously observe $\hat{\overline{T}}$ during the scan, (3) was evaluated using values of ϕ determined by the scanning mirror orientation with respect to the feedhorn basis. Under these conditions, $\hat{\overline{T}}$ remains constant while $\hat{\overline{T}}_f$ changes significantly due to the polarizing nature of the water surface. The results of the experiment are shown in Figure 3. The predicted value of $\overline{T}$ based on radiative transfer calculations appears as the solid straight lines in Figure 3. A small systematic error (< 7 K) caused by mechanical misalignment of the scan mirror and feedhorn axis is noticeable in the graph of T_v and T_h. Otherwise, rotation of the feedhorn brightnesses is straightforward; the rotated brightnesses track the calculated vertical and horizontal brightnesses well.

References

[1] Parks, G.S., T.C. Fraschetti, D.C. Miller, "Microwave Precipitation Radiometer", Jet Propulsion Laboratory Study Report JPL D-5397, May 1, 1988.

[2] Gasiewski, A.J. "A Technique for Measuring Vertically and Horizontally Polarized Brightness Temperatures Using Electronic Polarization Basis Rotation", Proceedings of the 1990 IEEE International Geoscience and Remote Sensing Symposium (IGARSS), pp. 1569-1572, May, 1990.

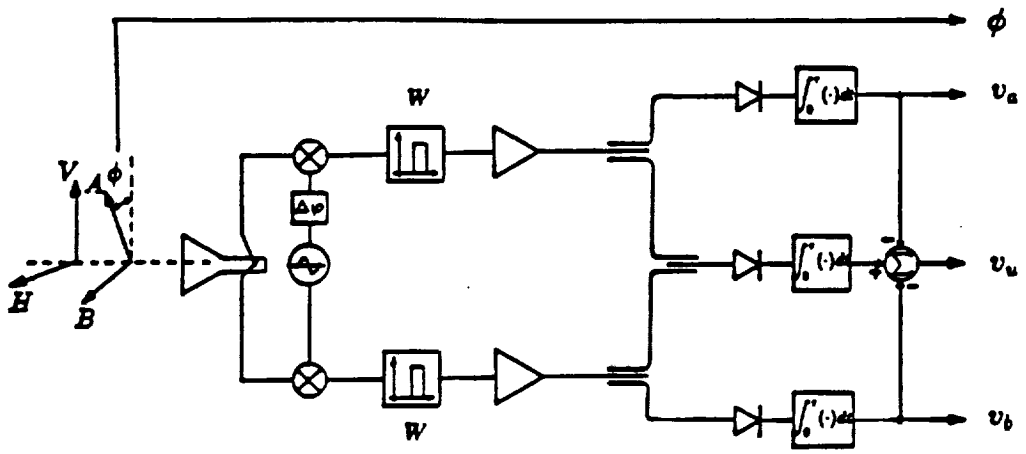

Figure 1: Block diagram of the 3-channel (T_A, T_U and T_B) radiometer used to implement electronic polarization basis rotation.

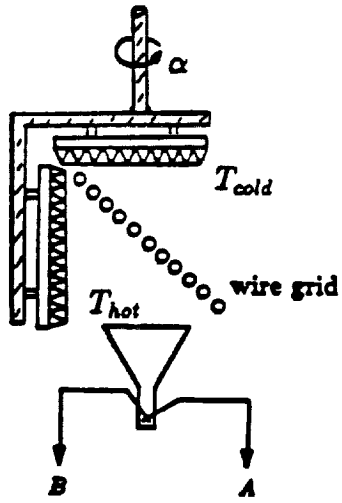

Figure 2: Schematic of the dual-polarized calibration load used to calibrate the 3-channel radiometer

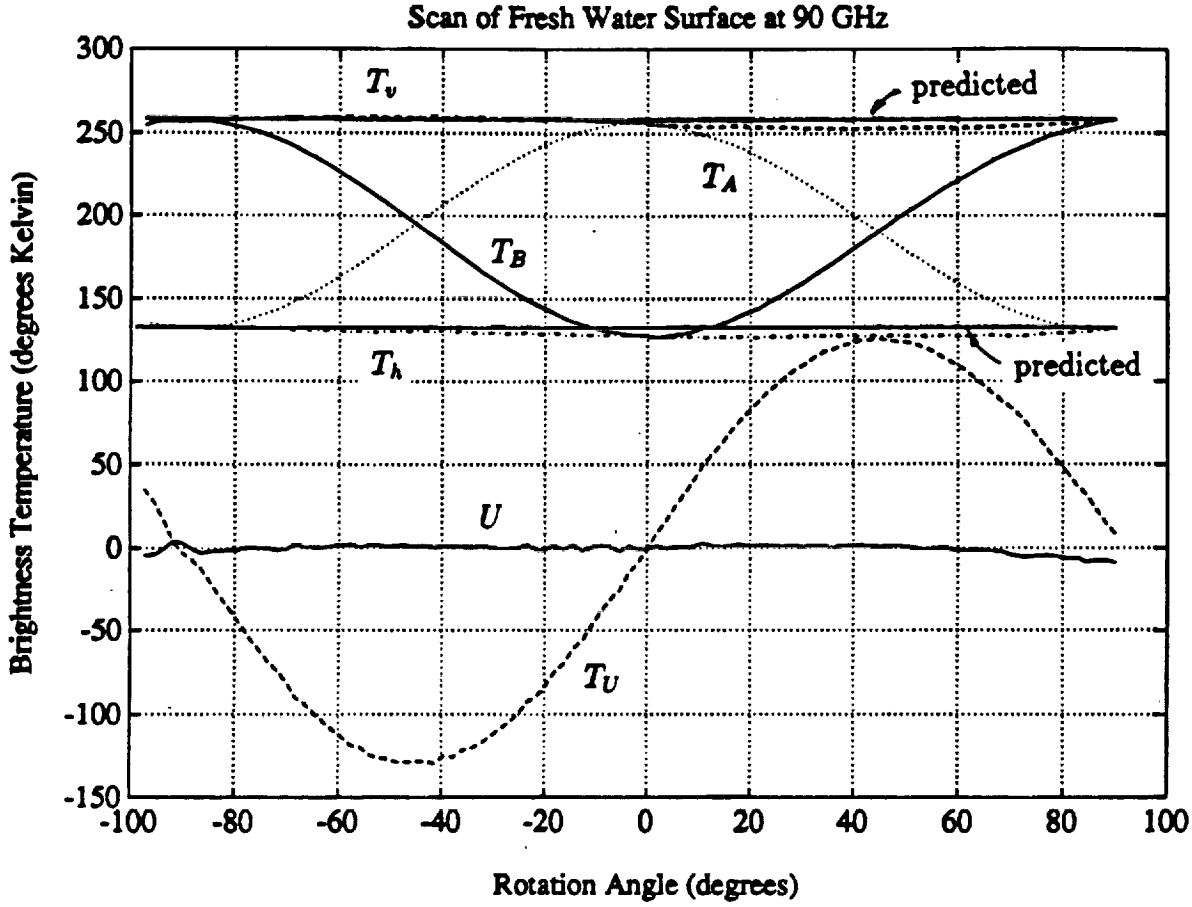

Figure 3: Scan of a fresh water surface using the 3-channel radiometer. The parameters T_A, T_U and T_B are the measured feedhorn brightness temperatures; T_v, T_h and U are estimates of the brightness temperatures in the Earth's vertical and horizontal basis. The predicted values of T_v and T_h from a numerical radiative transfer model are illustrated by the heavy straight lines.